

A LIGHT SUPERSYMMETRIC HIGGS SECTOR HIDDEN BY A STANDARD MODEL-LIKE HIGGS

Antonio Delgado^a, Germano Nardini^b, and Mariano Quiros^c

^a*Department of Physics, University of Notre Dame,
Notre Dame, IN 46556, USA*

^b*Fakultät für Physik, Universität Bielefeld, D-33615 Bielefeld, Germany*

^c*Institució Catalana de Recerca i Estudis Avançats (ICREA) and
Institut de Física d'Altes Energies, Universitat Autònoma de Barcelona
08193 Bellaterra, Barcelona, Spain*

Abstract

Extending the Higgs sector of the MSSM by triplets alleviates the little hierarchy problem and naturally allows for enhancements in the diphoton decay rate of the lightest CP-even Higgs h . In the present paper we analyze in detail the Higgs phenomenology of this theory with $m_h \simeq 126$ GeV. We mostly focus on a light Higgs sector where the pseudoscalar A , the next-to-lightest CP-even scalar H and the charged H^\pm Higgses are naturally at the electroweak scale. It turns out that for any value $m_A \gtrsim m_h$ there is a parameter region at small $\tan\beta$ where the CP-even Higgs sector appears at colliders as the SM one, except for loop-induced corrections. Notably the existence of this SM-like point, which is absent in the MSSM, is shared with supersymmetric theories where there are extra singlets. We also highlight a second parameter region at small m_A and small $\tan\beta$ where the h signal strengths, diphoton channel included, are SM-like except those of bottoms and taus which can have at most a 10-15% splitting. Improvements in the A and H^\pm searches are worthwhile in order to discriminate this scenario from the SM.

1 Introduction

The ATLAS and CMS collaborations at CERN are currently finding no clear discrepancies between the collected data and the predictions of the Standard Model (SM) with a Higgs mass around 126 GeV [1, 2]. Any firm conclusion about the lack of relevant new physics in the LHC data is however impossible because of the experimental uncertainties still being too large at present. Many theoretical works have thus elaborated plausible SM extensions in view that some of the present experimental anomalies will be confirmed with less statistical error, as for instance the $\gamma\gamma$, bb and $\tau\tau$ Higgs rates. In this sense many efforts have been made to extend the SM [3–7] or to look for appropriate parameter regions in the minimal (MSSM) or non-minimal supersymmetric SM extensions [8–12], as those including extra singlets (NMSSM) [13–18] and triplets [19–21] (or even in the presence of effective operators beyond the MSSM [22]), whose original motivation, besides adjusting the LHC data, is to solve the hierarchy problem.

Although the MSSM solves the hierarchy problem, i.e. it provides a technical solution to the existence of a grand hierarchy between the GUT (or Planck) and the electroweak scales, it requires an (unpleasant) amount of fine tuning in the electroweak sector in order to reproduce the 125-126 GeV Higgs mass, the so-called little hierarchy problem. Non-minimal supersymmetric scenarios generically alleviate the little hierarchy problem since they provide an extra tree-level contribution to the SM-like Higgs mass which makes the theory less dependent on large radiative corrections and, in turn, on large values of the supersymmetry breaking scale. If one keeps the SM group $SU(3)_c \otimes SU(2)_L \otimes U(1)_Y$ as the gauge symmetry of the theory the only remaining possibility (assuming renormalizable couplings) is to introduce an extra sector of chiral superfields coupled to the MSSM Higgs sector in the superpotential. These extended models are then limited to involving only extra singlets and/or triplets with hypercharges $Y = 0, \pm 1$ [23, 24]. In comparison with singlet extensions, models with triplets present the extra bonus of having new charginos which can be strongly (but perturbatively) coupled to the Higgs sector and may radiatively rise the $\gamma\gamma$ production rate above the SM prediction. Therefore, if these radiative corrections are small, as for instance when the new charginos are heavy enough, the phenomenology of the model is expected to be similar to that of supersymmetric theories with extra singlets weakly mixed with Higgs doublets.

The simplest of such a MSSM extension, i.e. a $Y = 0$ triplet coupled to the Higgs sector with a superpotential coupling λ , was investigated in Ref. [20] in the decoupling limit, i.e. for the CP-odd Higgs mass m_A much larger than the electroweak scale. In this case the tree-level couplings of the lightest Higgs h to the SM particles equal those of the SM and the major potential signature of the model is an enhancement in processes mediated by charginos, in particular the decay rate of the $h \rightarrow \gamma\gamma$ channel [20]. The decoupling regime however introduces a sizeable amount of fine-tuning in the model as, in the minimization conditions of the Higgs potential, cancellations of $\mathcal{O}(m_A^2)$ terms are required to fix the Z boson squared mass m_Z^2 to its experimental value. It is therefore compelling to abandon the decoupling regime and consider m_A at the electroweak scale.

In this paper we make a detailed study of the $Y = 0$ triplet extension of the MSSM,

for a value of the light Higgs mass $m_h \simeq 126$ GeV in the non-decoupling regime, where the masses of the remaining MSSM Higgs scalars (H, A, H^\pm) are at the electroweak scale. Stops and scalar triplets are instead assumed at the TeV scale in agreement with collider and electroweak precision observables [25], and so their radiative corrections to the Higgs production and decay rates are consequently small [20, 26]. The most striking result of the paper is that for any value of $m_A \gtrsim m_h$ there is a SM-like point at $\tan\beta = \tan\beta_c$ and $\lambda = \lambda_c$ (whose explicit value depends on the rest of supersymmetric parameters) where the tree-level Higgs couplings g_{hXX} (with $X = W, Z, b, t, \tau$, where b, t, τ stand respectively for down quarks, up quarks and charged leptons of the three families) equal the SM values and only a departure in the branching ratio of $h \rightarrow \gamma\gamma$, as large as 40%, can appear depending on the chargino spectrum. This means that the region around the SM-like point is consistent with actual experimental data. Given the present large experimental uncertainties no attempt has been made to fit the ATLAS and CMS measurements, a task which will be compelling in the future when experimental data will be more precise. Moreover, depending on the value of m_A , there can exist a second point at $\lambda > \lambda_c$ where the couplings g_{hXX} ($X = t, W, Z, \gamma$) are similar to the SM ones, while there is a splitting between the bb and $\tau\tau$ channels produced by radiative corrections. The region around this point will also deserve a more detailed analysis when more accurate experimental data will be available.

The outlook of the paper is as follows. In section 2 we introduce the model. Its scalar sector (including the minimization conditions for the electroweak minimum and scalar masses including radiative corrections) and the chargino sector, which will be relevant for the diphoton production. In particular we pay particular attention to the appearance of the SM-like point already mentioned. In section 3 the Higgs coupling are presented and it is explicitly shown how the branching ratios of the $bb, \tau\tau, tt, WW$, and ZZ channels normalized to their SM values are precisely equal to one at the SM-like point for any value of $m_A \gtrsim m_h$ while the actual value for the $\gamma\gamma$ channel presents an enhancement with respect to the SM value depending on the spectrum of chargino masses. The Higgs production rates are analyzed in detail in section 4 where a particular example with $m_A = 140$ GeV is exhibited as a function of λ for both gluon-fusion and vector boson fusion production mechanisms. The appearance of the SM-like point, as well as the existence of the second point compatible with present experimental data, is made explicit. We also present results on the production of the next-to-lightest CP-even Higgs (with a mass around 140 GeV) that explain why this particle has been undetected in the present LHC data. All these results are obtained by means of an approximation dealing with the scalar triplet being decoupled from the Higgs doublets (fully justified if the scalar triplet is sufficiently heavy), which implies a tiny contribution to the T parameter triggered by the triplet vacuum expectation value (VEV), and in section 5 we check the accuracy of this approximation. We find that in our analysis the approximation leads to a theoretical error on the Higgs mass of ± 0.5 GeV, which is smaller than the expected uncertainty from unconsidered radiative contributions. On the other hand the error made in the determination of the Higgs couplings is less than 1%. Finally in section 6 we consider the full case where the triplet can be rather light and get mixed with the doublet scalars as much as the present experimental bounds on the T parameter allows for. Instead

of a general analysis, which is outside the scope of the present paper, we focus on the trajectory of the SM-like points corresponding to a scalar triplet mass decreasing from large to smaller values in agreement with electroweak constraints. It turns out that the maximum allowed value of the $\gamma\gamma$ production rate increases as the triplet scalar mass decreases and it can reach at most a 40% enhancement with respect to the SM value. Finally some technical details concerning the existence of the SM-like point are shown in the appendix.

2 The model

A $Y = 0$ triplet Σ is described by its electrically charged and neutral components, ξ_1^- , ξ_2^+ and ξ^0 , as

$$\Sigma = \begin{pmatrix} \xi^0/\sqrt{2} & -\xi_2^+ \\ \xi_1^- & -\xi^0/\sqrt{2} \end{pmatrix}. \quad (2.1)$$

The most general renormalizable superpotential that couples Σ to the Higgs sector is given by

$$\Delta W = \lambda H_1 \cdot \Sigma H_2 + \frac{1}{2} \mu_\Sigma \text{tr} \Sigma^2 + \mu H_1 \cdot H_2. \quad (2.2)$$

where $A \cdot B \equiv \epsilon_{ij} A^i B^j$ with $\epsilon_{21} = -\epsilon_{12} = 1$ and $\epsilon_{22} = \epsilon_{11} = 0$. In the superpotential the identity $\text{Tr}(\Sigma^3) \equiv 0$ prevents the presence of the cubic term involving ξ^0 and ξ^\pm . The new parameters (including soft terms) with respect to the MSSM are then, the superpotential coupling λ , the supersymmetric mass μ_Σ , the soft-breaking masses m_4 and B_Σ and the trilinear soft-breaking parameter A_λ , and we assume no CP violation in the Higgs sector.

2.1 The scalar triplet-Higgs sector

The tree-level potential for the neutral components of the Higgs and triplet sector, $H_{1,2}^0$ and ξ^0 , is given by ¹

$$\begin{aligned} V = & m_1^2 |H_1^0|^2 + m_2^2 |H_2^0|^2 + m_4^2 |\xi^0|^2 \\ & + \left| \mu H_2^0 - \lambda H_2^0 \xi^0 / \sqrt{2} \right|^2 + \left| \mu H_1^0 - \lambda H_1^0 \xi^0 / \sqrt{2} \right|^2 \\ & + \left| \mu_\Sigma \xi^0 - \lambda H_1^0 H_2^0 / \sqrt{2} \right|^2 + \frac{g^2 + g'^2}{8} (|H_2^0|^2 - |H_1^0|^2)^2 \\ & + \left(B_\Sigma \mu_\Sigma \xi^0 \xi^0 - A_\lambda \lambda H_1^0 H_2^0 \xi^0 / \sqrt{2} - m_3^2 H_1^0 H_2^0 + \text{h.c.} \right). \end{aligned} \quad (2.3)$$

The experimental bound on the T -parameter constrains the parameters of the potential. It requires the VEV of ξ^0 to be around or below the GeV scale. Unless there is a fine tuning,

¹The analysis of the full triplet-Higgs potential including the components ξ_1^- , ξ_2^+ , H_1^- and H_2^+ is quite cumbersome. It can be easily imposed however that the physical minimum where none of these electrically-charged fields acquires a VEV is stable or at least long-lived [24]. We can then carry out perturbation theory around this minimum.

this imposes the hierarchy (cf. e.g. Ref. [20])

$$|A_\lambda|, |\mu|, |\mu_\Sigma| \lesssim 10^{-2} \frac{m_\Sigma^2 + \lambda^2 v^2 / 2}{\lambda v}, \quad (2.4)$$

with $m_\Sigma^2 \equiv m_4^2 + \mu_\Sigma^2 + B_\Sigma \mu_\Sigma$. Such a hierarchy may naturally arise in some models of supersymmetry breaking. In particular in gauge mediation [27] the trilinear soft terms are loop suppressed with respect to soft breaking masses. Moreover if the scale of supersymmetry breaking is high enough and gauge interactions transmitting supersymmetry breaking are not the SM ones, gravitational interactions can solve the μ -problem while the long running can create hierarchies among different soft masses [28]. We will just assume this hierarchy in the rest of the paper and consequently the small ξ^0 VEV will be neglected.

Unlike in the MSSM, the D -flat direction $|H_1^0| = |H_2^0|$ (with $\xi^0 = 0$) is stable, independently of the values of the mass parameters, due to the term $(\lambda^2/2)|H_1^0 H_2^0|^2$ in the potential. This term also modifies the minimization conditions valid for the MSSM. In the vacuum, where $\langle H_1^0 \rangle = v_1$ and $\langle H_2^0 \rangle = v_2$, the (tree-level) potential (2.3) provides the correct electroweak symmetry breaking if the following equalities are fulfilled:

$$m_3^2 = m_A^2 \sin \beta \cos \beta, \quad (2.5)$$

$$m_Z^2 = \frac{m_2^2 - m_1^2}{\cos 2\beta} - m_A^2 + \frac{\lambda^2}{2} v^2, \quad (2.6)$$

$$m_A^2 = m_1^2 + m_2^2 + 2|\mu|^2 + \frac{\lambda^2}{2} v^2, \quad (2.7)$$

where $\tan \beta = v_2/v_1$, $v = \sqrt{v_1^2 + v_2^2} = 174$ GeV, and m_Z is the Z boson mass.

By the definitions $H_i^0 = v_i + (h_i + i\chi_i)/\sqrt{2}$ and $x = \text{Re } \xi^0/\sqrt{2}$, the CP-even scalar squared mass matrix can be written as

$$\frac{1}{2}(h_2, h_1, x) \widehat{\mathcal{M}}^2 \begin{pmatrix} h_2 \\ h_1 \\ x \end{pmatrix} \quad \text{with} \quad \widehat{\mathcal{M}}^2 = \begin{pmatrix} & & \cdot \\ \mathcal{M}^2 & & \cdot \\ \cdot & \cdot & m_\Sigma^2 + \frac{\lambda^2}{2} v^2 \end{pmatrix}, \quad (2.8)$$

where \mathcal{M}^2 is, at tree level, given by

$$\mathcal{M}_0^2 = \begin{pmatrix} m_A^2 \cos^2 \beta + m_Z^2 \sin^2 \beta & (\lambda^2 v^2 - m_A^2 - m_Z^2) \sin \beta \cos \beta \\ (\lambda^2 v^2 - m_A^2 - m_Z^2) \sin \beta \cos \beta & m_A^2 \sin^2 \beta + m_Z^2 \cos^2 \beta \end{pmatrix}. \quad (2.9)$$

The entries represented by dots are terms typically of $\mathcal{O}(\lambda \hat{\mu} v)$, with $\hat{\mu} = \max\{|\mu|, |\mu_\Sigma|, |A_\lambda|\}$. If they are negligible with respect to $m_\Sigma^2 + \lambda^2 v^2 / 2$, the diagonalization of $\widehat{\mathcal{M}}^2$ is practically independent of them and no mixing is present between the CP-even Higgs sector of the MSSM and the triplet. Moreover, under such a hierarchy, a similar splitting between the triplet and the CP-odd and charged MSSM Higgs sectors also holds². It then turns out that the phenomenology of the model can be described by quite simple analytic expressions since:

²For explicit expressions of the corresponding mass matrices see e.g. Ref. [24, 26].

i) β is the rotation angle diagonalizing the CP-odd and charged Higgs squared-mass matrices, like in the MSSM; *ii)* The parameter m_A^2 defined in eq. (2.7) is the tree-level squared mass of the lightest CP-odd Higgs, and; *iii)* The tree-level mass of the lightest charged Higgs H^\pm can be easily expressed as ³

$$m_{H^\pm}^2 = m_A^2 + m_W^2 + \frac{\lambda^2}{2}v^2 . \quad (2.10)$$

In order to understand analytically the main features of the considered scenario we will focus on regimes where the entries $\mathcal{O}(\lambda\hat{\mu}v)$ in eq. (2.8) can be ignored. Notice that neglecting these off-diagonal terms leads to overestimating the lightest eigenvalue of the squared mass matrix in eq. (2.8), m_h^2 , by a correction of order of $\lambda^2\hat{\mu}^2v^2/(m_\Sigma^2m_h^2)$. *For the sake of comprehension* the present analysis will thus focus on values of m_Σ^2 that are sufficiently large to *safely* ensure this correction to be negligible. Specifically for $\mu = \mu_\Sigma = 250$ GeV and $A_\lambda = 0$, the overestimate on $m_h = 126$ GeV is below 1 GeV when $m_\Sigma \gtrsim 5$ TeV ⁴. This parameter setting is widely consistent with the bound (2.4), which would already be fulfilled at $m_\Sigma \gtrsim 1.5$ TeV. For the sake of analytic tractability, however, we take hereafter $m_\Sigma = 5$ TeV (with $\mu = \mu_\Sigma = 250$ GeV and $A_\lambda = 0$).

Of course the matrix \mathcal{M}^2 differs from \mathcal{M}_0^2 by radiative corrections, which also modify the tree-level minimization conditions (2.6) and (2.7). We will consider radiative corrections coming from fields strongly coupled to the Higgs sector (but still in the perturbative regime) and with large supersymmetry breaking masses, providing radiative corrections enhanced by large enough logarithms (but still consistent with the validity of the one-loop approximation). The most relevant contributions are generated by the stop ⁵ and triplet ⁶ sectors. Their radiative corrections can be computed by means of the one-loop effective potential in the presence of the $H_{1,2}^0$ background fields. Neglecting the Higgs-triplet mixing and assuming $m_\Sigma^2 \gg B_\Sigma\mu_\Sigma$, the background fields generate the following scalar triplet and stop spectrum (at order λ^2 and h_t^2):

$$\begin{aligned} m_{\xi^0}^2 &= m_\Sigma^2 + \frac{\lambda^2}{2} \left(|H_1^0|^2 + |H_2^0|^2 \right) , \\ m_{\xi_2^+}^2 &= m_\Sigma^2 + \lambda^2 |H_2^0|^2 , \\ m_{\xi_1^-}^2 &= m_\Sigma^2 + \lambda^2 |H_1^0|^2 , \\ m_{\tilde{t}}^2 &= m_Q^2 + h_t^2 |H_2^0|^2 , \end{aligned} \quad (2.11)$$

³Note that the λ^2 -term in eq. (2.10) provides a positive contribution to $m_{H^\pm}^2$, unlike in singlet extensions of the MSSM. Therefore experimental lower limits on m_{H^\pm} [29–32] do not put any upper bound on λ as a function of m_A .

⁴These values of μ and μ_Σ are chosen in view of the Higgs diphoton rate enhancement and chargino bounds studied in section 3. The 1 GeV estimate is instead obtained in the analysis of section 5 including radiative corrections.

⁵Corrections due to the sbottom sector are subleading in the phenomenologically interesting cases $\tan\beta \ll m_t/m_b$, where m_t and m_b are the top and bottom quark masses, respectively.

⁶Corrections coming from the Higgs sector are suppressed, with respect to those of the triplet, by small logarithms and they are then neglected throughout this paper.

where $h_t = m_t/(v \sin \beta)$ and the parameters μ and A_t are assumed to be much smaller than the (common) stop supersymmetry breaking mass m_Q .

By expanding the one-loop effective potential with the above stop and triplet spectrum, it turns out that the tree-level minimization conditions (2.7) have to be corrected by the amount

$$\Delta m_A^2 = \frac{3\lambda^2}{16\pi^2} m_\Sigma^2 (t_\Sigma - 1) + \frac{3h_t^2}{8\pi^2} m_Q^2 (t_Q - 1) , \quad (2.12)$$

with $t_\Sigma \simeq \log(m_\Sigma^2/\mu_\Sigma^2)$ and $t_Q = \log(m_Q^2/m_t^2)$. In the same way, m_Z^2 is given by expression (2.6), where m_A^2 includes the radiative correction (2.12), plus the genuine radiative contribution

$$\Delta m_Z^2 = -\frac{\lambda^4}{16\pi^2} v^2 t_\Sigma + \frac{6h_t^2}{16\pi^2} \frac{m_Q^2}{\cos 2\beta} (t_Q - 1) . \quad (2.13)$$

Moreover from the triplet sector the matrix \mathcal{M}_0^2 receives the radiative contributions

$$\begin{aligned} \Delta_\Sigma \mathcal{M}_{11}^2 &= \frac{5\lambda^4}{32\pi^2} t_\Sigma v^2 \sin^2 \beta , \\ \Delta_\Sigma \mathcal{M}_{22}^2 &= \frac{5\lambda^4}{32\pi^2} t_\Sigma v^2 \cos^2 \beta , \\ \Delta_\Sigma \mathcal{M}_{12}^2 &= \frac{\lambda^4}{32\pi^2} t_\Sigma v^2 \sin \beta \cos \beta , \end{aligned} \quad (2.14)$$

while the stop sector provides the corrections ⁷

$$\begin{aligned} \Delta_{\bar{t}} \mathcal{M}_{11}^2 &= \frac{3}{8\pi^2} t_Q h_t^2 \sin^2 \beta \left[-m_Z^2 + 2h_t^2 v^2 \left(1 + \frac{t_Q}{16\pi^2} \left(\frac{3h_t^2}{2} - 8g_3^2 \right) \right) \right] , \\ \Delta_{\bar{t}} \mathcal{M}_{12}^2 &= \Delta_{\bar{t}} \mathcal{M}_{21}^2 = \frac{3}{16\pi^2} h_t^2 \sin \beta \cos \beta m_Z^2 t_Q . \end{aligned} \quad (2.15)$$

The amount of fine tuning present in this scenario is very sensitive to the choice of m_Σ^2 , specially through the radiative corrections to m_A^2 . Indeed, the percent fine-tuning of m_A^2 with respect to m_Σ^2 , which is defined as $100(\partial \log m_\Sigma^2 / \partial \log m_A^2)$, does ameliorate from around 2% to 40% by lowering m_Σ from 5 to 1.5 TeV (for $m_A = \mu_\Sigma = 250$ GeV). However, since our main conclusions, obtained for $m_\Sigma = 5$ TeV, also cover more natural choices of m_Σ (see section 6) we perform the analysis at $m_\Sigma = 5$ TeV keeping in mind that the fine tuning of the scenario could be easily reduced by decreasing m_Σ ⁸.

On the other hand, m_Z^2 is little sensitive to m_Σ^2 once m_A has been set (Δm_Z^2 is just logarithmically dependent on m_Σ). In order to fix m_Z^2 to its experimental value only a tuning due to m_Q^2 is then required, and naturalness criterion consequently drives m_Q to its

⁷In $\Delta_{\bar{t}} \mathcal{M}_{11}^2$ and $\Delta_{\bar{t}} \mathcal{M}_{12}^2$ some subleading terms are included for completeness (cf. e.g. [33]). We instead omit $\Delta_{\bar{t}} \mathcal{M}_{22}^2$ since it is negligible when $|\mu|^2, |A_t|^2 \ll m_Q^2$ as bottom Yukawa, hypercharge and weak coupling contributions are subdominant to radiative corrections proportional to λ and h_t (both close to one in the parameter space we will be interested in).

⁸We cannot consider $m_\Sigma \gg 5$ TeV in the one-loop approximation. For that case we should improve the triplet radiative corrections in order to avoid perturbative problems.

lower bound coming from direct searches of stops [unlike in the MSSM, here the constraint $m_h \simeq 126$ GeV does not impose a stringent bound on m_Q^2 (even for $A_t = 0$) because of the tree-level interaction $\lambda^2 |H_1|^2 |H_2|^2$]. As a rather natural value, in the rest of the paper we take $m_Q = m_U = 700$ GeV, which is in full agreement with experimental constraints if gluinos are not light [34].

In summary, and unless explicitly specified, the parameter setting considered in this analysis is

$$\begin{aligned} m_Q = m_U = 700 \text{ GeV} , \quad A_t = 0 , \quad m_\Sigma = 5 \text{ TeV} , \\ \mu = \mu_\Sigma = 250 \text{ GeV} , \quad |M_3| = 1 \text{ TeV} . \end{aligned} \quad (2.16)$$

2.2 The constraint $m_h \simeq 126$ GeV and the SM-like point

In view of the recent ATLAS and CMS results [1, 2] we impose in the model the constraint that the lightest Higgs boson mass is around 126 GeV⁹. As discussed in section 2.1 the two lightest eigenstates of the squared mass matrix in eq. (2.8) are practically orthogonal to ξ_0 for large enough m_Σ^2 . They have masses

$$m_{h,H}^2 = \frac{1}{2} (\mathcal{T} \mp \Delta) \quad (2.17)$$

with

$$\mathcal{T} = \text{tr } \mathcal{M}^2 , \quad \Delta = \sqrt{\mathcal{T}^2 - 4\mathcal{D}} , \quad \mathcal{D} = \det \mathcal{M}^2 , \quad (2.18)$$

and they are related to the original fields as

$$\begin{pmatrix} h_2 \\ h_1 \end{pmatrix} = \begin{pmatrix} \cos \alpha & \sin \alpha \\ -\sin \alpha & \cos \alpha \end{pmatrix} \begin{pmatrix} h \\ H \end{pmatrix} \quad (2.19)$$

where the mixing angle α is determined by

$$\sin 2\alpha = \frac{2\mathcal{M}_{12}^2}{\Delta} , \quad \cos 2\alpha = \frac{\mathcal{M}_{22}^2 - \mathcal{M}_{11}^2}{\Delta} . \quad (2.20)$$

Once one fixes m_A , the constraint $m_h = 126$ GeV in eq. (2.17) provides a relation between $\tan \beta$ and λ . The curves satisfying this relation are plotted in Fig. 1 (left panel) for several fixed values of m_A [the above stop and triplet radiative corrections are included in \mathcal{M} and evaluated for the parameter setting (2.16)]. The function $\beta = \beta(\lambda; m_A)$ is bivalued and we represent with a thick (thin) line the solution branch corresponding to larger (smaller) value of $\tan \beta$. We will use this function to implement the condition $m_h = 126$ GeV in the

⁹Several studies have investigated scenarios where the observed excess corresponds to the next-to-lightest Higgs while the lightest one (with a mass ~ 100 GeV) has not been detected yet [35]. Although this possibility is appealing, and can certainly be accommodated in our model, here we restrict our analysis to the more conservative assumption that ATLAS and CMS collaborations have discovered the lightest (CP-even) Higgs eigenstate.

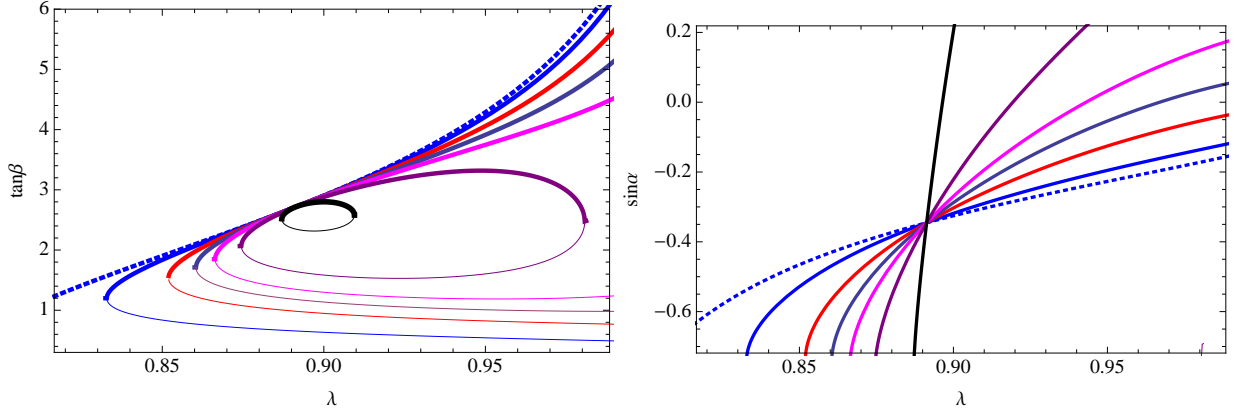


Figure 1: *Left panel: $\tan \beta$ as a function of λ providing $m_h = 126$ GeV in the decoupling limit or large m_A (blue dotted) and for $m_A = 200$ GeV (blue solid), 155 GeV (red solid), 145 GeV (grey solid), 140 GeV (magenta solid), 135 GeV (purple solid) and 130 GeV (black solid). The other parameter inputs are those of eq. (2.16). Right panel: The same but for $\sin \alpha$ as a function of λ .*

following observables, and we will plot them with thick (thin) lines when they correspond to the solution branch with larger (smaller) values of $\tan \beta$.

Independently of m_A , all lines intersect at the point

$$\tan \beta_c \simeq 2.72 \quad , \quad \lambda_c \simeq 0.89 \quad . \quad (2.21)$$

At such point the rotation angle diagonalizing \mathcal{M}^2 is independent of m_A^2 (see Fig. 1, right panel). Since this point (also) belongs to the line $m_A \rightarrow \infty$, the usual decoupling-limit relation $\alpha_c = \beta_c - \pi/2$ is satisfied at small m_A as well, and the tree-level couplings of the Higgs h to the SM particles are hence those of the SM. For this reason the parameter region around $(\tan \beta_c, \lambda_c)$ might provide a phenomenology very similar to the one of the SM (as discussed in the next sections, relevant differences may consist in the h diphoton and invisible channels, and in the A, H^0, H^\pm decays if m_A is light).

We can understand the origin of the *intersection point* (2.21) as follows. The function $\beta = \beta(\lambda; m_A)$ in the left panel of Fig. 1 is the solution of the following equation [cf. also eq. (2.17)] for a fixed value of m_h , in particular for $m_h = 126$ GeV:

$$\mathcal{D} - m_h^2 \mathcal{T} + m_h^4 = 0 \quad . \quad (2.22)$$

Eq. (2.22) is a first order polynomial in m_A^2 (the coefficient of m_A^4 cancels out) which can then be written as

$$A(\tan \beta, \lambda) m_A^2 + B(\tan \beta, \lambda) = 0 \quad . \quad (2.23)$$

For the point $(\tan \beta_c, \lambda_c)$ such that

$$\begin{cases} A(\tan \beta_c, \lambda_c) = 0 \\ B(\tan \beta_c, \lambda_c) = 0 \end{cases} \quad (2.24)$$

eq. (2.23) [and (2.22)] is fulfilled for any m_A , and any solution $\beta = \beta(\lambda; m_A)$ then crosses this point (for the given m_h and independently of m_A ¹⁰).

It is straightforward to find the analytical solution of the system (2.24) for the tree-level squared mass \mathcal{M}_0^2 . It is given by $\tan \beta_c^0 = 1$ and $\lambda_c^0 = \sqrt{2}m_h/v \simeq 1.02$, and one can easily check that $\alpha_c^0 = \beta_c^0 - \pi/2$ diagonalizes \mathcal{M}_0^2 . In the presence of radiative corrections the analytic solution is more cumbersome. It can be found in the Appendix and yields the critical values quoted in eq. (2.21). As the analytic expressions show, the dependence of $\tan \beta_c$ and λ_c on stop and triplet mass parameters is mild due to logarithmic suppressions and, in general, the larger these mass parameters the lower λ_c and the higher $\tan \beta_c$ (see Section 6 for a numerical example which in particular yields $0.85 \lesssim \lambda_c \lesssim 1$ and $1.5 \lesssim \tan \beta_c \lesssim 3$ as typical values). Let us finally comment that Eq. (2.24) does not have a solution in the MSSM. On the contrary, in theories with an extra quartic coupling in the tree-level potential, as the present model containing the additional triplet or even in theories with extra singlets, there can be in general a solution which implies the existence of the discussed SM-like intersection point.

3 The Higgs couplings

The angle α plays a fundamental role in the interactions of the CP-even Higgses with the SM fields, as shown in Table 1 where the ratios $r_{\mathcal{H}XX}^0$ are the tree-level approximation of the quantities [33]

$$r_{\mathcal{H}XX} = \frac{g_{\mathcal{H}XX}}{g_{\mathcal{H}XX}^{\text{SM}}} \quad \text{with} \quad \mathcal{H} = h, H; \quad X = W, Z, t, b, \tau, \quad (3.1)$$

being $g_{\mathcal{H}XX}$ and $g_{\mathcal{H}XX}^{\text{SM}}$ the (effective) couplings in the present theory and the SM, respectively.

The tree-level ratios r_{htt}^0 , $r_{hbb}^0 = r_{h\tau\tau}^0$ and $r_{hVV}^0 \equiv r_{hWW}^0 = r_{hZZ}^0$ are plotted in Fig. 2 for fixed values of m_A and along the curves $\beta = \beta(\lambda; m_A)$ of Fig. 1. As explained above, all

$r_{hWW}^0 = r_{hZZ}^0$	$r_{HWW}^0 = r_{HZZ}^0$	r_{htt}^0	r_{Htt}^0	$r_{hbb}^0 = r_{h\tau\tau}^0$	$r_{Hbb}^0 = r_{H\tau\tau}^0$
$\sin(\beta - \alpha)$	$\cos(\beta - \alpha)$	$\frac{\cos \alpha}{\sin \beta}$	$\frac{\sin \alpha}{\sin \beta}$	$-\frac{\sin \alpha}{\cos \beta}$	$\frac{\cos \alpha}{\cos \beta}$

Table 1: *The tree-level value of ratios (3.1) for the different channels.*

¹⁰Had we included the (small) radiative corrections stemming from the Higgs sector the solution to eq. (2.24) $(\tan \beta_c, \lambda_c)$ would exhibit a tiny inappreciable (logarithmic) dependence on m_A which we are neglecting throughout this paper.

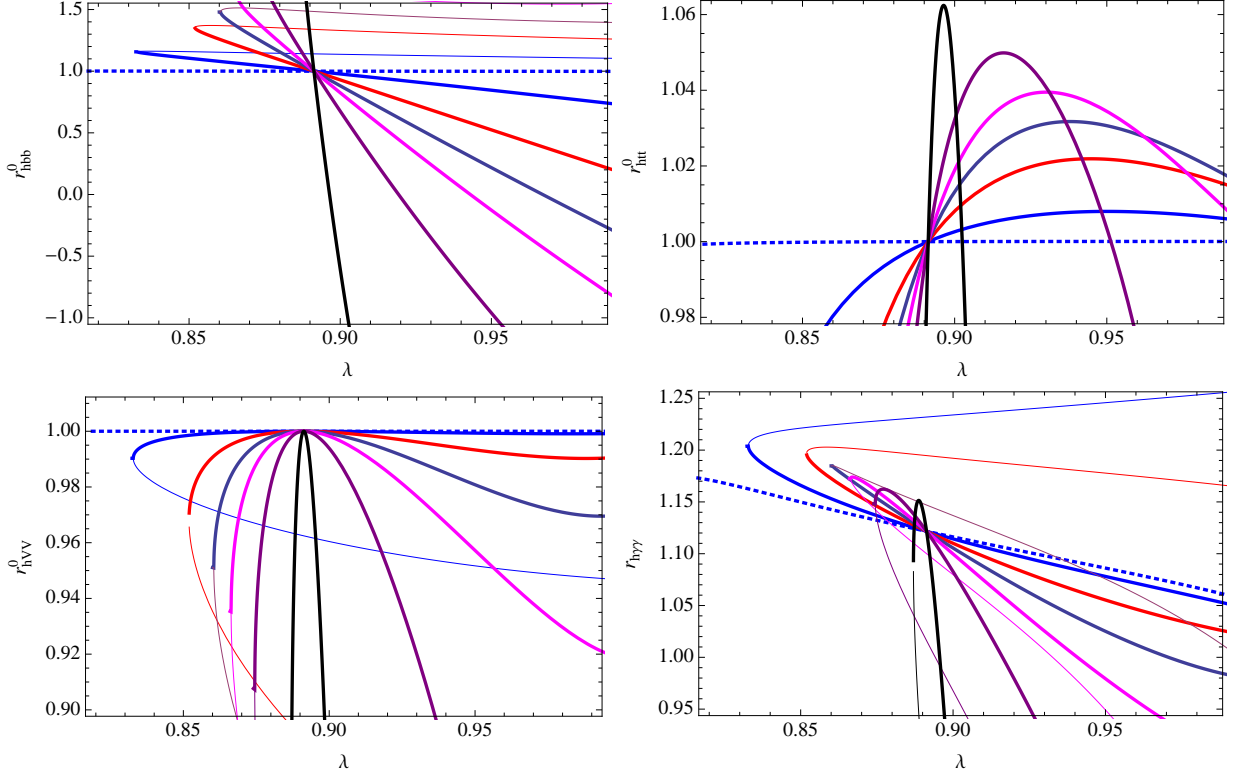


Figure 2: Plot of the normalized tree-level couplings r_{hbb}^0 (upper left panel), r_{htt}^0 (upper right panel) and r_{hVV}^0 (lower left panel) and one-loop effective coupling $r_{h\gamma\gamma}$ (lower right panel) as a function of λ for different values of m_A . The constraints $m_h = 126$ GeV, $m_{\chi_{1\pm}} = 104$ GeV and setting (2.16) are assumed. Thick (thin) lines correspond to the large (small) $\tan\beta$ branch in Fig. 1. Colour code is the same as in Fig. 1.

of them are equal to one at the intersection value $(\tan\beta_c, \lambda_c)$. In particular this is so for r_{hbb}^0 (Fig. 2 left upper panel). However moving away from the intersection point one can easily modify r_{hbb}^0 by $\mathcal{O}(\pm 1)$ factors, depending on the values of m_A . On the other hand for either sufficiently large m_A (decoupling region) or for parameter points near the SM-like intersection point $(\tan\beta_c, \lambda_c)$, the bb and $\tau\tau$ production via Higgs decays, which respectively behave like $(r_{hbb}^0)^2$ and $(r_{h\tau\tau}^0)^2$ at leading order, may appear in very good agreement with the SM predictions, provided that the other couplings take values close enough to the SM ones (more details will be given in section 4).

Radiative corrections can of course induce important modifications to the tree-level couplings. In particular, because of sbottom-gluino (stop-gluino) loops, the ratio r_{hbb}^0 (r_{htt}^0) gets

renormalized as [36]

$$\begin{aligned} r_{hbb} &= r_{hbb}^0 \left[1 - \frac{\Delta(m_b)}{1 + \Delta(m_b)} \left(1 + \frac{1}{\tan \alpha \tan \beta} \right) \right], \\ r_{htt} &= r_{htt}^0 \left[1 - \frac{\Delta(m_t)}{1 + \Delta(m_t)} (1 + \tan \alpha \tan \beta) \right], \end{aligned} \quad (3.2)$$

with

$$\begin{aligned} \Delta(m_b) &= \frac{2\alpha_3}{3\pi} \tan \beta M_3 \mu f(m_{\tilde{b}}, M_3), \\ \Delta(m_t) &= \frac{2\alpha_3}{3\pi \tan \beta} M_3 \mu f(m_{\tilde{t}}, M_3), \\ f(x, y) &= \frac{x^2 - y^2 + y^2 \log y^2/x^2}{(x^2 - y^2)^2}, \end{aligned} \quad (3.3)$$

where M_3 and $m_{\tilde{b}}$ are respectively the gluino and sbottom masses (in the sbottom sector we consider $m_D = m_Q$ and $A_b = 0$). The couplings g_{htt} and g_{hbb} may then depart from the corresponding SM values in the presence of rather light gluinos and third generation squarks. The same effect does not instead arise for the decays involving the τ leptons and first two generation quarks because of the small $\tan \beta$ regime imposed by the requirement $m_h = 126 \text{ GeV}$ (cf. left panel of Fig. 1). In Higgs search data these radiative corrections might be an important signature to discriminate experimentally the SM from the present triplet scenario if its parameters are close enough to the intersection point, the remaining Higgses cannot be detected and charginos are relatively heavy (i.e. if there is no sizeable Higgs diphoton enhancement, as we will discuss next).

Radiative corrections are also crucial for loop-induced decays. Charginos can provide sizeable contributions to $g_{\mathcal{H}\gamma\gamma}$ in addition to those of the top and W boson already present in the SM. Because of the electrically-charged triplet fermions, the effective coupling $g_{h\gamma\gamma}$ can be enhanced much more than in the MSSM¹¹, even though it does not differ from the SM coupling if charginos are heavy or from the MSSM one if μ_Σ is large and λ is small. The consequent increasing of $\Gamma(h \rightarrow \gamma\gamma)$ has been already studied in the decoupling limit [20] and here we extend that analysis to more general cases.

The chargino sector already contained in the MSSM ($\tilde{W}^\pm, \tilde{H}_1^-, \tilde{H}_2^+$) mixes with the triplet charginos ($\tilde{\xi}_1^-, \tilde{\xi}_2^+$). Their mass matrix is given by

$$\left(\tilde{W}^-, \tilde{H}_1^-, \tilde{\xi}_1^- \right) \mathcal{M}_{1/2}^\pm \begin{pmatrix} \tilde{W}^+ \\ \tilde{H}_2^+ \\ \tilde{\xi}_2^+ \end{pmatrix}, \quad \mathcal{M}_{1/2}^\pm = \begin{pmatrix} M_2 & gv_2 & 0 \\ gv_1 & \mu & -\lambda v_2 \\ 0 & -\lambda v_1 & \mu_\Sigma \end{pmatrix}, \quad (3.4)$$

and their contribution to $g_{\mathcal{H}\gamma\gamma}$ can be determined from the QED effective potential [4, 37, 38]

$$\mathcal{L}_{\gamma\gamma}^{1/2} = F_{\mu\nu}^2 \frac{\alpha}{16\pi} 2b_{1/2} \log \det \mathcal{M}_{1/2}^\pm (v_i + h_i/\sqrt{2}), \quad (3.5)$$

¹¹ For an earlier analysis see Ref. [26].

with $b_{1/2} = 4/3$. By expanding $\mathcal{L}_{\gamma\gamma}^{1/2}$ to linear order in h_i and projecting onto the Higgs eigenstates h, H one obtains

$$\begin{aligned}
r_{h\gamma\gamma} &= \frac{A_1(\tau_W) \sin(\beta - \alpha) + b_{1/2} A_{1/2}(\tau_t) \frac{\cos \alpha}{\sin \beta} + \frac{b_{1/2} \cos(\alpha + \beta) v^2 (M_2 \lambda^2 + g^2 \mu_\Sigma)}{\sin \beta \cos \beta v^2 (M_2 \lambda^2 + g^2 \mu_\Sigma) - M_2 \mu \mu_\Sigma}}{A_1(\tau_W) + b_{1/2} A_{1/2}(\tau_t)} \\
r_{H\gamma\gamma} &= \frac{A_1(\tau_W) \cos(\beta - \alpha) + b_{1/2} A_{1/2}(\tau_t) \frac{\sin \alpha}{\sin \beta} + \frac{b_{1/2} \sin(\alpha + \beta) v^2 (M_2 \lambda^2 + g^2 \mu_\Sigma)}{\sin \beta \cos \beta v^2 (M_2 \lambda^2 + g^2 \mu_\Sigma) - M_2 \mu \mu_\Sigma}}{A_1(\tau_W) + b_{1/2} A_{1/2}(\tau_t)}
\end{aligned} \tag{3.6}$$

where $A_1(\tau_W) \simeq -8.3$ and $A_{1/2}(\tau_t) \simeq 1.4$. Eq. (3.6), which reproduces the result of Ref. [20] in the decoupling limit, shows that large enhancements can arise due to charginos. The exact amount of increase depends on many parameters which might be constrained by future searches at the LHC. For instance, in order to fulfill the chargino mass bound $m_{\tilde{\chi}_1^\pm} \gtrsim 104 \text{ GeV}$ [25] with any sensible value of λ , one has to choose $|\mu|$ and $|\mu_\Sigma|$ similar to (or larger than) those we are considering in this analysis. In the following we impose $m_{\tilde{\chi}_1^\pm} = 104 \text{ GeV}$ which, in turn, determines the value of M_2 along the curves $\beta = \beta(\lambda; m_A)$ of Fig. 1. In particular it implies $M_2(\tan \beta_c, \lambda_c) \simeq 164 \text{ GeV}$ for our setting (2.16). Moreover at the intersection point (2.21) $r_{h\gamma\gamma}$ has to coincide for all the curves $\beta(\lambda; m_A)$, independently of m_A , as a glance at expression (3.6) suggests and Fig. 2 (right lower panel) clearly confirms. Notice that at the intersection point, which depends on our parameter choice, the enhancement is $r_{h\gamma\gamma}(\tan \beta_c, \lambda_c) \simeq 1.12$, but for smaller m_Σ (larger $|\mu|$ and $|\mu_\Sigma|$) a larger (smaller) $r_{h\gamma\gamma}$ at the new intersection point is possible. More details on this issue will be presented in section 6.

4 Higgs production rates at the LHC

From the values of $r_{\mathcal{H}XX}$ determined in the previous section one can compute the predicted signal strength $\mathcal{R}_{\mathcal{H}XX}$ of the decay channel $\mathcal{H} \rightarrow XX$, with $\mathcal{H} = h, H$ and $X = W, Z, t, b, \tau$:

$$\mathcal{R}_{\mathcal{H}XX} = \frac{\sigma(pp \rightarrow \mathcal{H}) BR(\mathcal{H} \rightarrow XX)}{[\sigma(pp \rightarrow h) BR(h \rightarrow XX)]_{SM}}. \tag{4.1}$$

In particular for the gluon-fusion (ggF), the associated production with heavy quarks ($\mathcal{H}tt$), the associated production with vector bosons ($V\mathcal{H}$) and the vector boson fusion (VBF) production processes, one can write

$$\begin{aligned}
\mathcal{R}_{\mathcal{H}XX}^{(ggF)} &= \mathcal{R}_{\mathcal{H}XX}^{(\mathcal{H}tt)} = \frac{r_{\mathcal{H}tt}^2 r_{\mathcal{H}XX}^2}{\mathcal{D}}, & \mathcal{R}_{\mathcal{H}XX}^{(VBF)} &= \mathcal{R}_{\mathcal{H}XX}^{(V\mathcal{H})} = \frac{r_{\mathcal{H}WW}^2 r_{\mathcal{H}XX}^2}{\mathcal{D}}, \\
\mathcal{D} &= BR(h \rightarrow b\bar{b})_{SM} r_{\mathcal{H}bb}^2 + BR(h \rightarrow gg, cc)_{SM} r_{\mathcal{H}tt}^2 \\
&+ BR(h \rightarrow \tau\tau)_{SM} r_{\mathcal{H}\tau\tau}^2 + BR(h \rightarrow WW, ZZ)_{SM} r_{\mathcal{H}WW}^2,
\end{aligned} \tag{4.2}$$

where we assume that: *i*) $\Gamma(\mathcal{H} \rightarrow gg)$ is dominated by the top loop so that $r_{\mathcal{H}gg} = r_{\mathcal{H}tt}$ ¹²,

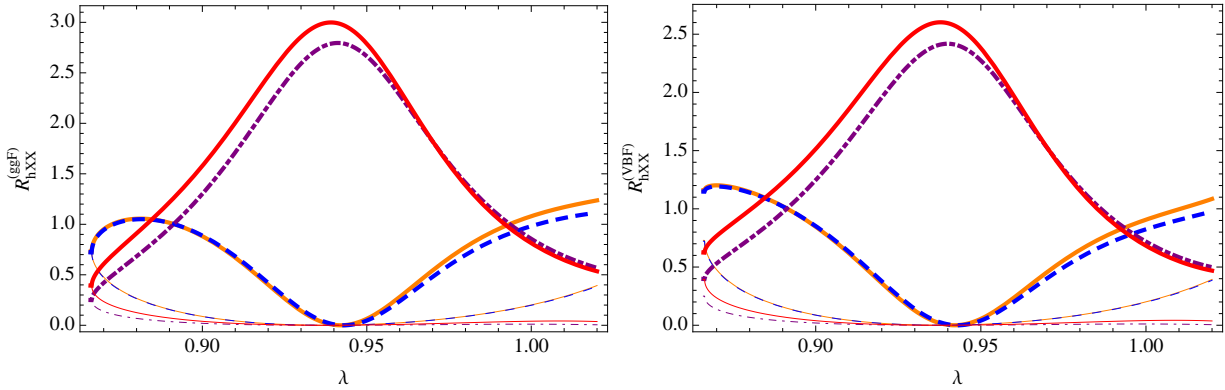


Figure 3: *Left panel: Signal strengths for the lightest Higgs production by the gluon-fusion mechanism followed by decay in different channels: $\mathcal{R}_{hbb}^{(ggF)}$ (solid orange line), $\mathcal{R}_{h\tau\tau}$ (dashed blue line), \mathcal{R}_{hWW} (dot dashed purple line) and $\mathcal{R}_{h\gamma\gamma}$ (solid red line), for $m_A = 140$ GeV. The constraints $m_h = 126$ GeV, $m_{\chi_1^\pm} = 104$ GeV and setting (2.16) are implemented. Thick (thin) lines correspond to the large (small) $\tan\beta$ branch in Fig. 1. Right panel: The same but for the vector boson fusion production.*

which requires for instance that there is no light colored supersymmetric particle (e.g. light stop) strongly coupled to the Higgs; *ii*) the invisible decay width of \mathcal{H} into neutralinos is negligible¹³.

Besides the Higgs diphoton width, in the decoupling limit all branching ratios of h are in quite good agreement with those of the SM (unless there are rare large radiative corrections in bb and tt channels), which are $BR(h \rightarrow bb)_{SM} = 0.56$, $BR(h \rightarrow \tau\tau)_{SM} = 0.06$, $BR(h \rightarrow WW, ZZ)_{SM} = 0.26$, $BR(h \rightarrow gg, cc)_{SM} = 0.11$ at $m_h = 126$ GeV (we also take $\Gamma_{SM} = 4.2$ MeV) [40]. The phenomenology of this case has been studied in Ref. [20]¹⁴ for large values of m_A . In this paper we instead focus on the regime of small m_A . As discussed below, the presence of light A , H and H^\pm might be the key signature to distinguish the triplet scenario from the SM at the LHC.

For $m_A = 140$ GeV the behavior of the signal strengths \mathcal{R}_{hXX} along the curves $\beta(\lambda; m_A)$ of Fig. 1 are exhibited in Fig. 3. The decays originated by gluon (vector boson) fusion Higgs production are presented in the left (right) panel of the figure. As we can see, only thick lines, which correspond to the larger- $\tan\beta$ branch of solutions in Fig. 1, are phenomenologically relevant if one requires the LHC observed excess to be related only to the lightest Higgs, as we do in this paper. We have fixed the relative signs of μ and M_3 such that $sign(\mu M_3) < 0$.

¹²However, when $r_{\mathcal{H}tt} \ll 1$, as it can be the case for the Higgs H , we consider also the correction from the bottom loop and then $r_{Hgg}^2 = [r_{Htt} + (m_b/m_t)r_{Hbb}]^2$.

¹³For a study where both assumptions are violated and the interplay between light stops and neutralinos is crucial to reproduce the LHC data, see e.g. Ref. [39].

¹⁴Some numerical discrepancies may be detected between the analysis of Ref. [20] and the present one which are due to the use of different inputs.

Because of this assignment, bb versus $\tau\tau$ production is enhanced at $\lambda \gtrsim 0.95$. Had we chosen $sign(\mu M_3) > 0$ the bb (solid orange) curve would underlie the $\tau\tau$ (blue dashed) line. On the other hand, different choices of M_3 and $m_{\tilde{t}}$ could have slightly increased or largely suppressed the relative enhancement with respect to the case plotted in Fig. 3. Moreover notice that $\Delta(m_b)$ generates a relatively small splitting between bb and $\tau\tau$ channels, especially at the intersection point (2.21), indicating *a posteriori* that radiative corrections which are subleading to $\Delta(m_b)$ are negligible, as we are assuming in this analysis.

An important issue highlighted in Fig. 3 is the possibility of having SM-like production and decay rates in the small- m_A regime. At the intersection point (2.21) *the signal strengths of $bb, \tau\tau, WW$ and ZZ channels are as in the SM* (unless of subleading corrections that can be modulated by different choices of the spectrum), with the notable difference of an about 25% excess in the diphoton Higgs decay, which could be reduced for larger values of chargino masses or increased for smaller values of m_Σ , as discussed in section 6. Therefore values of $(\tan\beta, \lambda)$ near $(\tan\beta_c, \lambda_c)$, as well as in the peculiar region around $(\tan\beta, \lambda) = (4.6, 0.995)$ of Fig. 3, seem the most promising to adjust future experimental data once their statistical and systematic uncertainties had been reduced ¹⁵.

The main feature of the peculiar region arising around $\lambda = 0.995$ for $m_A = 140$ GeV (it also exists for other small values of m_A) is that $\tan\beta$ is relatively large and $\sin\alpha/\cos\beta = \mathcal{O}(1)$ (cf. Figs. 1 and 2). The production of WW, ZZ therefore reproduces the one predicted in the SM. The diphoton signal strength is also SM-like because the enhancement due to charginos is suppressed by the relatively large value of $\tan\beta$ yielding small $\cos(\alpha + \beta)$ (α is positive and $\tan\alpha \simeq 1/\tan\beta$). Finally the production of bb is enhanced with respect to the $\tau\tau$ production because the radiative correction $\Delta(m_b)$ is proportional to $\tan\beta$. However, as stressed above, this relative enhancement can be reversed by changing $sign(M_3\mu)$ or can be made tiny for other values of $m_{\tilde{t}}, \mu$ and M_3 . In any case in this parameter region the model predicts $h \rightarrow \tau\tau$ rates that tend to be suppressed with respect to the SM in every Higgs production channel.

A last remark on the region with large values of λ (namely $\lambda \gtrsim 0.95$ for $m_A = 140$ GeV): the signs of g_{hbb} and $g_{h\tau\tau}$ are opposite to those in the SM but their absolute values are close to 1 [cf. Fig. 2; notice also that the small radiative correction in eq. (3.2) does not flip the sign of g_{hbb}]. These unusual signs are not ruled out in the regime $\tan\beta \ll m_t/m_b$ that emerges in Fig. 1. In such a case, indeed, the absolute values of the couplings g_{hbb} and $g_{h\tau\tau}$ are much smaller than the top-quark Yukawa coupling, and interference in observables sensitive to either $sign(g_{hbb})$ or $sign(g_{h\tau\tau})$ are difficult to detect (unlike the case of $sign(g_{htt})$, see e.g. Ref. [41]).

On the other hand even in the SM-like intersection region with all \mathcal{R}_{hXX} equal to 1 (but m_A small), one can try to discriminate the SM from this scenario by looking at the remaining Higgs fields whose masses are in the energy range probed by the LHC. Focusing first on the field H , its mass m_H as a function of λ at $m_A = 140$ GeV is shown in the left

¹⁵We wish to stress here that the existence of the SM-like intersection point does not rely on the chosen values of the parameters, and different settings from that in eq. (2.16) would only influence the values of $(\tan\beta_c, \lambda_c)$ and consequently the amount of diphoton excess. The second peculiar point for $\lambda \simeq 1$ is instead strongly parameter dependent and only exists for small values of m_A .

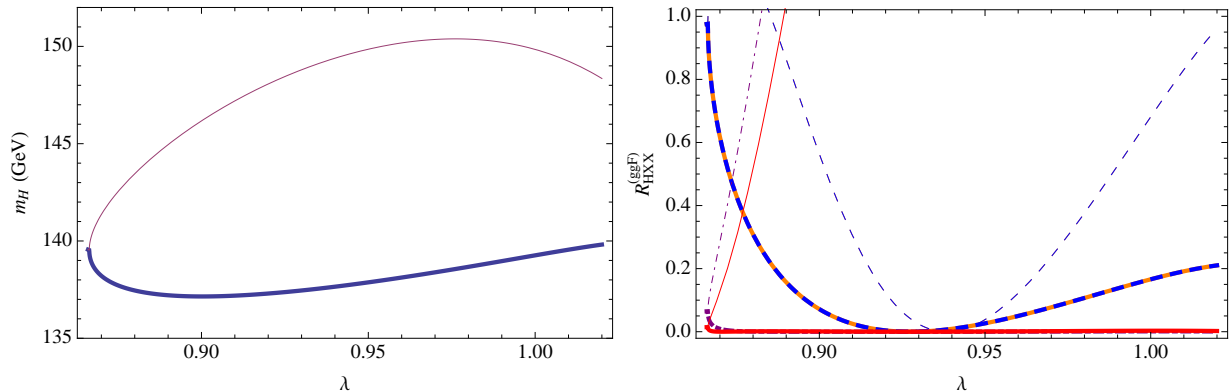


Figure 4: *Left panel: Plot of the next-to-lightest Higgs mass m_H as a function of λ for $m_A = 140$ GeV. The constraint $m_h = 126$ GeV and setting (2.16) are implemented. Thick (thin) lines correspond to the large (small) $\tan\beta$ branch in Fig. 1. Right panel: The same as in the left panel of Fig. 3 but for the next-to-lightest Higgs signal strengths $\mathcal{R}_{HXX}^{(ggF)}$ produced by gluon fusion.*

panel of Fig. 4. The thickness code is the same as in the previous figures. Since for the thin lines all signal strengths \mathcal{R}_{hXX} are very suppressed¹⁶, the phenomenologically relevant curves are the thick ones, which correspond to $m_H \simeq 139$ GeV. The field H has therefore small signal strengths \mathcal{R}_{HXX} at the values of λ providing realistic light-Higgs phenomenology [cf. Fig. 3]. In particular at the promising SM-like intersection point $\lambda \simeq \lambda_c$ the productions of WW , ZZ and $\gamma\gamma$ are unobservable and there is only a little fermion production with $\mathcal{R}_{H\tau\tau} \simeq \mathcal{R}_{Hbb} \simeq 0.1$. Furthermore, if the lightest neutralino was in the (short) mass range $m_h/2 < m_{\tilde{\chi}_1^0} < m_H/2$ the invisible channel $H \rightarrow \tilde{\chi}_1^0 \tilde{\chi}_1^0$ could further dilute the fermion branching ratios without altering the signal strengths \mathcal{R}_{hXX} . Looking for signatures of light A and H^\pm seems therefore more promising.

Quantifying the A and H^\pm field phenomenology is strongly parameter dependent and correlating it to the CP-even Higgs signatures would require dedicated analyses that we leave for future research. Nevertheless we can already envisage the main features since the A and H^\pm are expected to have signatures quite similar to those in the MSSM. Their couplings to the SM fields are indeed obtained by rotating by the angle β the CP-odd and charged components of $H_{1,2}$, like in the MSSM. The relevant difference is of course the mass spectrum. For instance, for the cases where we can find $\mathcal{R}_{hXX} \approx 1$, the relation $m_{H^\pm} > m_t$ arises at even relatively small m_A , unlike in the MSSM and its singlet extensions [cf. eq. (2.10)]. It thus escapes from the experimental constrains which focus on the possibility of the charged Higgs

¹⁶We remind the reader that we assume the field h to be the recently observed particle and the unique Higgs in the range $123 \text{ GeV} \lesssim m_h \lesssim 126 \text{ GeV}$. Other Higgs spectrum scenarios, such as for instance $m_h = 123 \text{ GeV}$ (or $m_h \ll 123 \text{ GeV}$) and $m_H = 126 \text{ GeV}$, would require a dedicated analysis which is beyond the scope of the present paper.

being produced as a decay of the top. The branching ratios $BR(H^\pm \rightarrow tb)$ and $BR(H^\pm \rightarrow \tau\nu_\tau)$ are then expected to be the dominant ones, possibly along with $BR(H^\pm \rightarrow \chi_1^0\chi_1^\pm)$ when the channel is kinematically accessible. Moreover, although strongly model dependent, some relevant constraints on the H^\pm radiative corrections are possible, e.g. the experimental measure of $B \rightarrow X_s\gamma$ is expected to bound the H^\pm versus χ_1^\pm space of parameters.

Also the CP-odd Higgs signatures should be basically similar to those in the MSSM. The field A is produced only through gluon fusion and decays mainly into bottom pairs. Its tree-level coupling to weak vector bosons is zero and its decay into photons is two orders of magnitude smaller than the one of h [42]. Moreover for the case $m_A = 140$ GeV that we have previously considered, the decay channel $A \rightarrow hZ$ is kinematically forbidden (it opens up at $m_A \gtrsim 217$ GeV). Understanding whether the decay products of a light A field appear in the LHC Higgs search analyses as particles produced by the h decay, and therefore whether our parameter regions around the intersection points are actually compatible with the reinterpreted experimental data for low m_A , would require a much more refined study than the one we have carried out here. In this sense we stress that the qualitative results we highlighted at $m_A = 140$ GeV, are also valid at m_A large enough not to introduce the above potential subtlety. On the other hand, the same problem would exist also in the MSSM. For this reason we expect that the experimental bounds on m_A and m_H^\pm in the present model are similar to those obtained in the MSSM¹⁷ from direct searches. In particular since CMS and ATLAS mainly focus on the bottom signal for the Higgs in association with a weak vector boson [1, 2], those bounds do not apply to the CP-odd Higgs as the latter is not produced in that channel.

5 Accuracy of the decoupling approximation

The results of the previous sections are obtained by neglecting the triplet-Higgs mixing terms in eq. (2.8). Here we check the goodness of this approximation for our choice $m_\Sigma = 5$ TeV. First of all let us remind that in all cases neglecting the VEV of the neutral triplet field ξ^0 in the minimization and squared-mass equations is a consequence of the experimental constraint on the T -parameter which imposes $m_\Sigma \gtrsim 1.5$ TeV if no parameter tuning is present. However for $m_\Sigma \sim 1.5$ TeV, although one can certainly neglect the value of $\langle \xi^0 \rangle$, one cannot ignore the matrix elements

$$\begin{aligned} \widehat{\mathcal{M}}_{31}^2 = \widehat{\mathcal{M}}_{13}^2 &= (E_2 \cos \beta + E_3 \sin \beta)v \\ \widehat{\mathcal{M}}_{32}^2 = \widehat{\mathcal{M}}_{23}^2 &= (E_3 \cos \beta + E_2 \sin \beta)v \end{aligned} \quad (5.1)$$

where

$$E_2 = -\frac{\lambda}{\sqrt{2}}(A_\lambda + \mu_\Sigma), \quad E_3 = -\sqrt{2}\lambda\mu, \quad (5.2)$$

which will modify the eigenvalues of the squared-mass matrix as well as the rotation angles

¹⁷Of course, only MSSM experimental bounds that do not make use of the constraint $m_h \approx 126$ GeV in the analysis should apply. For updated studies see talks in Ref. [43].

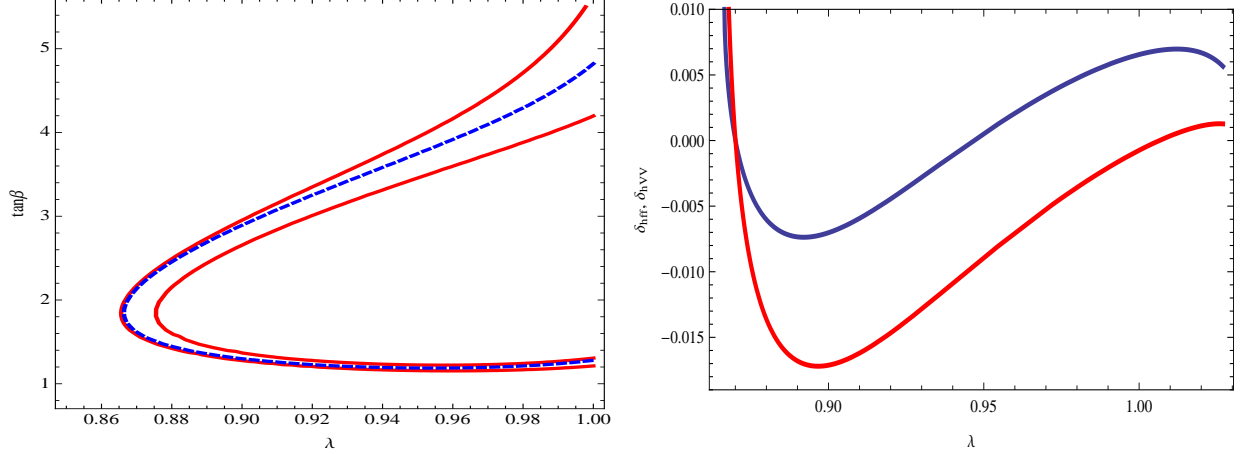


Figure 5: *Left panel: Contour plots in the $(\lambda, \tan\beta)$ plane for $m_h = 126$ GeV in the approximation of decoupling triplet scalars (blue dashed line) and $m_h = 125$ GeV (outer red solid line) and 126 GeV (inner red solid line) in the exact theory. Right panel: Plots of δ_{hff} (upper grey solid line) and δ_{hVV} (lower red solid line) as a function of λ along the dashed contour of the left panel.*

diagonalizing it, and thus the couplings of the CP-even Higgs sector to tt , bb , $\tau\tau$, WW , ZZ . In other words the experimental constraint on the T -parameter ($m_\Sigma \gtrsim 1.5$ TeV) is not strong enough to implement full decoupling of the triplet scalars. Instead, for $m_\Sigma = 5$ TeV the decoupling approximation that neglects the entries (5.1) is good enough, as we now check.

In the left panel of Fig. 5 we plot the constraint on λ and $\tan\beta$ coming from the requirement $m_h = 126$ GeV in the decoupling approximation (dashed blue line) with $m_A = 140$ GeV and the parameter setting (2.16). The curve lies in between the lines corresponding to $m_h = 125$ GeV (outer solid red line) and $m_h = 126$ GeV (inner solid red line) derived from the full squared-mass matrix $\widehat{\mathcal{M}}^2$. We see that the decoupling approximation at $m_\Sigma = 5$ TeV never overestimates the mass m_h by more than 1 GeV, which is well within the theoretical uncertainties of our calculation of the lightest Higgs mass and the experimental errors in the determination of the Higgs mass at the LHC. In particular the overestimate at $\lambda = \lambda_c$ could have been easily absorbed by shifting by about 1 GeV the input value of m_h in the approximated theory, i.e. from $m_h = 126$ GeV to $m_h = 127$ GeV.

Besides the overestimate on the lightest Higgs mass, one also has to check the error on the lightest-Higgs couplings. Their uncertainties are estimated in the right panel of Fig. 5 where, considering $\beta = \beta(\lambda)$ along the dashed line of the left panel (i.e. imposing $m_h = 126$ GeV in the approximated theory), we plot the quantities δ_{hff} ($f = b, t, \tau$) and δ_{hVV} ($V = W, Z$) defined as

$$\delta_{hXX} = \frac{r_{hXX}^{ex} - r_{hXX}^{ap}}{r_{hXX}^{ex}}, \quad (5.3)$$

where the superscript *ex* (*ap*) refers to the exact (decoupling approximation) results. In all the cases the approximated approach provides couplings with less than 1% error, which proves that the results of the previous sections are reliable as expected. Moreover we can see that $\delta_{hXX} = 0$ at $\lambda \simeq 0.86$ near, but not quite coincident with, the intersection point (2.21). This means, as we will see in detail in the next section, that the existence of the (SM-like) intersection point is not an artifact of the decoupling approximation [where $r_{hXX}^{ap}(\lambda_c^{ap}) = 1$] but also appears in the non-decoupled cases¹⁸ [where $r_{hXX}^{ex}(\lambda_c^{ex}) = 1$] although its localization is slightly shifted ($\lambda_c^{ex} \neq \lambda_c^{ap}$).

6 Some comments on the non-decoupling regime

As we have previously noticed the parameter m_Σ can be lowered down to values around 1.5 TeV, consistently with electroweak experimental observables. However in the low m_Σ region allowed by the experimental constraint on the T parameter, neglecting the off-diagonal matrix entries (5.1) is a rude approximation, as one can explicitly check. One then should study the model by a full numerical analysis which is outside the scope of the present paper. Instead we can easily investigate the low- m_Σ scenario at the (phenomenologically interesting) intersection points fixing the Higgs mass $m_h = 126$ GeV in the exact theory. At the intersection point, indeed, the lightest-Higgs production and decay rates are at tree-level those of the SM, and the effect of moving m_Σ translates just in a modification of the actual value of $(\lambda_c, \tan \beta_c)$ which the one-loop Higgs rates depend on (there is no explicit dependence on m_Σ).

The position of the intersection point in the $(\lambda, \tan \beta)$ plane as a function of m_Σ can be easily deduced from the left panel of Fig. 6. For a given point of the m_Σ curve (dotted line), the point in the solid line having the same abscissa gives the coordinates $(\lambda_c, \tan \beta_c)$ of the intersection point in the scenario with that particular value of m_Σ . As already explained, departures of \mathcal{R}_{hXX} from one (with X a SM particle) appear at the intersection points only via loop effects. In particular the Higgs diphoton channel is extremely sensitive to the changes in $(\lambda_c, \tan \beta_c)$ caused by modifications of m_Σ [cf. eq. (3.6)]. This is quantified in the right panel of Fig. 6 where one can read the value of $\mathcal{R}_{h\gamma\gamma}$ at the intersection point for different values of m_Σ by comparing the left and right panels of the figure. For instance, looking at the solid curve of the right panel (i.e. $m_{\chi_1^\pm} = 104$ GeV with $\mu = \mu_\Sigma = 250$ GeV), for $m_\Sigma = 1.5$ TeV the $h \rightarrow \gamma\gamma$ decay rate is about 1.4 times larger than in SM at the intersection point, which corresponds to $\lambda_c \simeq 1$ and $\tan \beta_c \simeq 1.8$. However, the diphoton excess decreases by raising the chargino spectrum. In particular at the intersection point for $m_\Sigma = 1.5$ TeV it turns out that $\mathcal{R}_{h\gamma\gamma} = 1.25$ for $m_{\chi_1^\pm} = 150$ GeV, with $\mu = \mu_\Sigma = 300$ GeV (dashed line), and $\mathcal{R}_{h\gamma\gamma} = 1.16$ for $m_{\chi_1^\pm} = 200$ GeV, with $\mu = \mu_\Sigma = 350$ GeV (dotted line). As expected, in the limit of large $m_{\chi_1^\pm}$ the diphoton signal strength at the intersection point approaches unity. Moreover, once the chargino spectrum is fixed, the maximum $\mathcal{R}_{h\gamma\gamma}$ occurs

¹⁸This fact can be easily related to the cancellation of the m_A^4 term in eq. (2.22) which in turn implies that m_h^2 is not controlled by supersymmetry breaking parameters in the decoupling limit of the most general supersymmetric theory, but by the electroweak breaking scale v^2 .

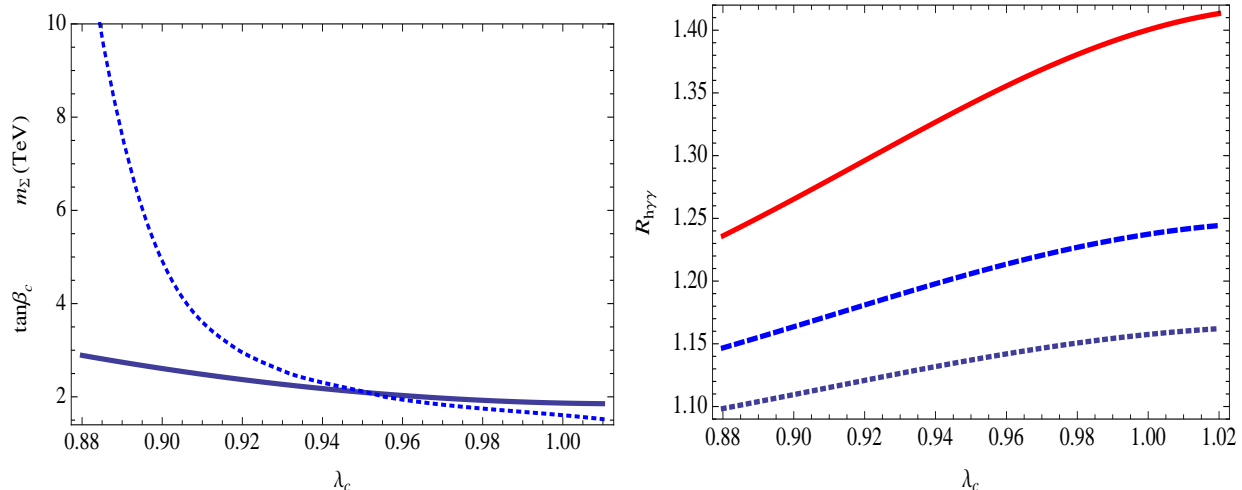


Figure 6: *Left panel: Values of $(\tan \beta_c, \lambda_c)$ (solid line) for m_Σ in the range $1.5 \text{ TeV} \leq m_\Sigma \leq 10 \text{ TeV}$ (dotted line). The 126 GeV constraint on the lightest Higgs mass in the exact theory, the setting (2.16) (except for m_Σ) is implemented. Right panel: The corresponding value of $\mathcal{R}_{h\gamma\gamma}$ as a function of λ_c along the intersection points for the different values of m_Σ and the requirements $m_{\chi_1^\pm} = 104 \text{ GeV}$ (solid line), $m_{\chi_1^\pm} = 150 \text{ GeV}$ with $\mu = \mu_\Sigma = 300 \text{ GeV}$ (dashed line) and $m_{\chi_1^\pm} = 200 \text{ GeV}$ with $\mu = \mu_\Sigma = 350 \text{ GeV}$ (dotted line).*

for the lowest possible value of m_Σ because it allows the lowest (highest) possible value of $\tan \beta_c$ (λ_c) compatible with the fixed value of m_h .

In summary from this brief analysis at low m_Σ it seems that rather large diphoton enhancements can arise in the most natural frameworks (i.e. m_Σ small, as discussed in section 2.1). However, achieving a firm conclusion on the naturalness of a large diphoton excess would only be possible by a numerical study on the tuning needed in the chargino parameters (constrained by the T -parameter bound) and on the low- m_Σ phenomenology occurring at $(\lambda, \tan \beta)$ different from the intersection point.

7 Conclusion

In view of the actual value of the Higgs mass provided by the ATLAS and CMS experiments at the LHC, the MSSM as a solution to the hierarchy problem loses part of its naturalness (as the theory requires heavy stops and large mixing) and thus develops a little hierarchy problem. A way to alleviate this issue is to enlarge the MSSM field content by singlets and/or triplets strongly (but perturbatively) coupled to the Higgs sector as they introduce additional tree-level contributions to the SM-like Higgs mass. On top of that triplets can also increase the $\gamma\gamma$ Higgs branching ratio by means of extra chargino loops in the process $h \rightarrow \gamma\gamma$, in agreement with recent data on diphoton production at the LHC. This fact was explicitly exhibited in a previous publication [20] focusing on the decoupling regime,

i.e. assuming the next-to-lightest CP-even (H) and the lightest CP-odd (A) Higgses much heavier than the electroweak scale. In this regime the tree-level couplings in the decay rates $h \rightarrow bb, \tau\tau, tt, WW, ZZ$ equal the SM ones and only the departure of the process $h \rightarrow \gamma\gamma$ is relevant. However, on the one hand the decoupling regime (where m_A is much larger than the electroweak scale) introduces an extra *inherent fine-tuning* as cancellations between $\mathcal{O}(m_A^2)$ terms are required to fix m_Z^2 to its experimental value. On the other hand in the decoupling limit the SM-like Higgs is indistinguishable from the SM one in the channels dominated by the tree-level Higgs decays (only channels generated by loop corrections are modified) while *the extra Higgs sector is very heavy and thus difficult to detect*. These features make it interesting to consider the non-decoupling regime of supersymmetric theories.

In this paper we have considered the non-decoupling regime of the theory where a zero hypercharge triplet superfield is added to the MSSM. In this case, in which all the Higgs sector is light and within the LHC energy range, the issue concerning the phenomenological feasibility of the model is two-fold:

- i)* The prediction for $\sigma(pp \rightarrow h)BR(h \rightarrow XX)$ should be in agreement with the experimental data at the LHC. It should then not deviate too much from the SM prediction, possibly except for the diphoton channel.
- ii)* The prediction for $\sigma(pp \rightarrow H)BR(H \rightarrow XX)$ should explain why the state H (if kinematically accessible at the LHC) has not been detected.

Requirement *i)* has been positively fulfilled as in the considered theory there is, for any value of m_A , a SM-like point at small $\tan\beta$ (whose value depends on the other supersymmetric parameters) for which all couplings between h and the SM fields equal the corresponding SM ones. Similar properties also arise in a second peculiar point which however seems to exist only for some specific choice of m_A and supersymmetric parameters. Notably, the SM-like point does not exist in the MSSM but in principle it does in theories where singlets and/or triplets with non-zero hypercharge are introduced. Therefore all signal strengths of decay rates proceeding by tree-level diagrams satisfy the condition $\sigma(pp \rightarrow h)BR(h \rightarrow XX) \simeq \sigma_{SM}(pp \rightarrow h)BR_{SM}(h \rightarrow XX)$ and thus they are in good agreement with experimental data. Large modifications can instead appear in branching ratios of loop-induced processes, as e.g. in the diphoton channel where we can find some large enhancement with respect to the SM result, depending on the chargino mass spectrum. As the value of the couplings of h and H to various final states are correlated we find strong suppressions of $\sigma(pp \rightarrow H)BR(H \rightarrow XX)$ which can solve the issue *ii)* above. In fact we have found that the only relevant production rates are for $H \rightarrow bb, \tau\tau$ which are less than 10% the values expected in the SM for a Higgs of the same mass, and which might eventually be discovered at the high luminosity LHC14 or in a future linear collider.

Of course once we have opened Pandora's box of a light scalar sector there are other processes which should be investigated, in particular those involving the pseudoscalar A and charged H^\pm Higgses, especially the former which is the lightest one. We have only briefly discussed some of the possible signatures for production and decay of A and H^\pm , partly due to the absence of experimental data for these particles. However a dedicated study, both

theoretical and experimental, covering this region is worth in the future when more data concerning the Higgs sector will be accumulated at the LHC.

ACKNOWLEDGMENTS

GN and MQ thank the ICTP for hospitality during the first stages of this work. AD was partly supported by the National Science Foundation under grant PHY-1215979. MQ was supported by the Spanish Consolider-Ingenio 2010 Programme CPAN (CSD2007-00042) and by CICYT-FEDER-FPA2008-01430 and FPA2011-25948.

Appendix

A Analytic expressions for the SM-like point

At one-loop the matrix \mathcal{M}^2 in eq. (2.8) can be written as

$$\mathcal{M}^2 = \begin{pmatrix} m_A^2 \cos^2 \beta + m_{11}^2 \sin^2 \beta & (-m_A^2 + m_{12}^2) \sin \beta \cos \beta \\ (-m_A^2 + m_{12}^2) \sin \beta \cos \beta & m_A^2 \sin^2 \beta + m_{22}^2 \cos^2 \beta \end{pmatrix}, \quad (\text{A.1})$$

where we have used the redefinitions

$$m_{12}^2 = \lambda^2 v^2 - m_Z^2 + \Delta_{\tilde{t}} \mathcal{M}_{12}^2 + \Delta_{\Sigma} \mathcal{M}_{12}^2, \quad (\text{A.2})$$

$$m_{11}^2 = m_Z^2 + \Delta_{\tilde{t}} \mathcal{M}_{11}^2 + \Delta_{\Sigma} \mathcal{M}_{11}^2, \quad (\text{A.3})$$

$$m_{22}^2 = m_Z^2 + \Delta_{\Sigma} \mathcal{M}_{22}^2. \quad (\text{A.4})$$

It follows that the system of equations (2.24) turns out to be

$$\begin{cases} m_h^4 + \cos^2 \beta (m_h^2(m_{11}^2 - m_{22}^2) + \sin^2 \beta (m_{11}^2 m_{22}^2 - m_{12}^4)) - m_h^2 m_{11}^2 = 0 \\ -m_h^2 + m_{11}^2 \sin^4 \beta + (m_{22}^2 - 2m_{12}^2) \cos^4 \beta + 2m_{12}^2 \cos^2 \beta = 0 \end{cases} \quad (\text{A.5})$$

whence for $m_{12}^2 > 0$ one obtains

$$\begin{aligned} m_{12,c}^2 &= m_h^2 + \sqrt{(m_h^2 - m_{11}^2)(m_h^2 - m_{22}^2)}, \\ \cos^2 \beta_c &= \left(1 + \sqrt{\frac{m_h^2 - m_{22}^2}{m_h^2 - m_{11}^2}} \right)^{-1}. \end{aligned} \quad (\text{A.6})$$

Finally one can check analytically that the intersection points in the left and right panels of Fig. 1 correspond to the same parameter point. By using eq. (2.17) to express Δ in eq. (2.20), one observes that at the point (A.6) $\sin \alpha$ is independent of m_A and in particular, as it occurs in the decoupling limit $m_A \rightarrow \infty$, it is $\sin^2 \alpha_c = \cos^2 \beta_c$.

References

- [1] G. Aad *et al.* [ATLAS Collaboration], “Observation of a new particle in the search for the Standard Model Higgs boson with the ATLAS detector at the LHC,” Phys. Lett. B [arXiv:1207.7214 [hep-ex]].
- [2] S. Chatrchyan *et al.* [CMS Collaboration], “Observation of a new boson at a mass of 125 GeV with the CMS experiment at the LHC,” Phys. Lett. B [arXiv:1207.7235 [hep-ex]].
- [3] A. G. Akeroyd and S. Moretti, “Enhancement of H to gamma gamma from doubly charged scalars in the Higgs Triplet Model,” Phys. Rev. D **86** (2012) 035015 [arXiv:1206.0535 [hep-ph]].
- [4] M. Carena, I. Low and C. E. M. Wagner, “Implications of a Modified Higgs to Diphoton Decay Width,” arXiv:1206.1082 [hep-ph].
- [5] L. Wang and X. -F. Han, “130 GeV gamma-ray line and enhancement of $h \rightarrow \gamma\gamma$ in the Higgs triplet model plus a scalar dark matter,” Phys. Rev. D **87** (2013) 015015 [arXiv:1209.0376 [hep-ph]].
- [6] E. J. Chun, H. M. Lee and P. Sharma, “Vacuum Stability, Perturbativity, EWPD and Higgs-to-diphoton rate in Type II Seesaw Models,” JHEP **1211** (2012) 106 [arXiv:1209.1303 [hep-ph]].
- [7] M. Chala, “ $h \rightarrow \gamma\gamma$ excess and Dark Matter from Composite Higgs Models,” JHEP **1301** (2013) 122 [arXiv:1210.6208 [hep-ph]].
- [8] M. Carena, S. Gori, N. R. Shah, C. E. M. Wagner and L. -T. Wang, “Light Stau Phenomenology and the Higgs $\gamma\gamma$ Rate,” JHEP **1207** (2012) 175 [arXiv:1205.5842 [hep-ph]].
- [9] K. Schmidt-Hoberg and F. Staub, “Enhanced $h \rightarrow \gamma\gamma$ rate in MSSM singlet extensions,” JHEP **1210** (2012) 195 [arXiv:1208.1683 [hep-ph]].
- [10] T. Kitahara, “Vacuum Stability Constraints on the Enhancement of the $h \rightarrow \gamma\gamma$ rate in the MSSM,” JHEP **1211** (2012) 021 [arXiv:1208.4792 [hep-ph]].
- [11] L. Basso and F. Staub, “Enhancing $h \rightarrow \gamma\gamma$ with staus in SUSY models with extended gauge sector,” Phys. Rev. D **87** (2013) 015011 [arXiv:1210.7946 [hep-ph]].
- [12] R. Huo, G. Lee, A. M. Thalappilil and C. E. M. Wagner, “ $SU(2) \otimes SU(2)$ Gauge Extensions of the MSSM Revisited,” arXiv:1212.0560 [hep-ph].
- [13] U. Ellwanger, “A Higgs boson near 125 GeV with enhanced di-photon signal in the NMSSM,” JHEP **1203** (2012) 044 [arXiv:1112.3548 [hep-ph]].

- [14] J. -J. Cao, Z. -X. Heng, J. M. Yang, Y. -M. Zhang and J. -Y. Zhu, “A SM-like Higgs near 125 GeV in low energy SUSY: a comparative study for MSSM and NMSSM,” *JHEP* **1203** (2012) 086 [arXiv:1202.5821 [hep-ph]].
- [15] D. A. Vasquez, G. Belanger, C. Boehm, J. Da Silva, P. Richardson and C. Wymant, “The 125 GeV Higgs in the NMSSM in light of LHC results and astrophysics constraints,” *Phys. Rev. D* **86** (2012) 035023 [arXiv:1203.3446 [hep-ph]].
- [16] R. Benbrik, M. Gomez Bock, S. Heinemeyer, O. Stal, G. Weiglein and L. Zeune, *Eur. Phys. J. C* **72** (2012) 2171 [arXiv:1207.1096 [hep-ph]].
- [17] I. Gogoladze, B. He and Q. Shafi, “Inverse Seesaw in NMSSM and 126 GeV Higgs Boson,” *Phys. Lett. B* **718** (2013) 1008 [arXiv:1209.5984 [hep-ph]].
- [18] K. Choi, S. H. Im, K. S. Jeong and M. Yamaguchi, “Higgs mixing and diphoton rate enhancement in NMSSM models,” *JHEP* **1302** (2013) 090 [arXiv:1211.0875 [hep-ph]].
- [19] T. Basak and S. Mohanty, “Triplet-Singlet Extension of the MSSM with a 125 GeV Higgs and Dark Matter,” *Phys. Rev. D* **86** (2012) 075031 [arXiv:1204.6592 [hep-ph]].
- [20] A. Delgado, G. Nardini and M. Quiros, “Large diphoton Higgs rates from supersymmetric triplets,” *Phys. Rev. D* **86** (2012) 115010 [arXiv:1207.6596 [hep-ph]].
- [21] Z. Kang, Y. Liu and G. -Z. Ning, “Highlights of Supersymmetric Hypercharge ± 1 Triplets,” arXiv:1301.2204 [hep-ph].
- [22] F. Boudjema and G. D. La Rochelle, “Supersymmetric Higgses beyond the MSSM: An update with flavour and Dark Matter constraints,” *Phys. Rev. D* **86** (2012) 115007 [arXiv:1208.1952 [hep-ph]].
- [23] J. R. Espinosa and M. Quiros, “On Higgs boson masses in nonminimal supersymmetric standard models,” *Phys. Lett. B* **279**, 92 (1992); J. R. Espinosa and M. Quiros, “Upper bounds on the lightest Higgs boson mass in general supersymmetric Standard Models,” *Phys. Lett. B* **302**, 51 (1993) [hep-ph/9212305]; G. L. Kane, C. F. Kolda and J. D. Wells, “Calculable upper limit on the mass of the lightest Higgs boson in any perturbatively valid supersymmetric theory,” *Phys. Rev. Lett.* **70**, 2686 (1993) [hep-ph/9210242]; J. R. Espinosa and M. Quiros, “Gauge unification and the supersymmetric light Higgs mass,” *Phys. Rev. Lett.* **81**, 516 (1998) [hep-ph/9804235].
- [24] J. R. Espinosa and M. Quiros, “Higgs triplets in the supersymmetric standard model,” *Nucl. Phys. B* **384** (1992) 113.
- [25] J. Beringer *et al.* [Particle Data Group Collaboration], “Review of particle physics,” *Phys. Rev. D* **86**, 0100001 (2012).
- [26] S. Di Chiara and K. Hsieh, “Triplet Extended Supersymmetric Standard Model,” *Phys. Rev. D* **78** (2008) 055016 [arXiv:0805.2623 [hep-ph]].

- [27] G. F. Giudice and R. Rattazzi, Phys. Rept. **322** (1999) 419 [hep-ph/9801271].
- [28] A. Delgado, G. Nardini and M. Quiros, JHEP **1204** (2012) 137 [arXiv:1201.5164 [hep-ph]].
- [29] A. Heister *et al.* [ALEPH Collaboration], “Search for charged Higgs bosons in e^+e^- collisions at energies up to $\sqrt{s} = 209\text{-GeV}$,” Phys. Lett. B **543** (2002) 1 [hep-ex/0207054].
- [30] S. Chatrchyan *et al.* [CMS Collaboration], “Search for a light charged Higgs boson in top quark decays in pp collisions at $\sqrt{s} = 7\text{ TeV}$,” JHEP **1207** (2012) 143 [arXiv:1205.5736 [hep-ex]].
- [31] G. Aad *et al.* [ATLAS Collaboration], “Search for charged Higgs bosons through the violation of lepton universality in $t\bar{t}$ events using pp collision data at $\sqrt{s} = 7\text{ TeV}$ with the ATLAS experiment,” arXiv:1212.3572 [hep-ex].
- [32] G. Aad *et al.* [ATLAS Collaboration], “Search for a light charged Higgs boson in the decay channel $H^+ \rightarrow c\bar{s}$ in $t\bar{t}$ events using pp collisions at $\sqrt{s} = 7\text{ TeV}$ with the ATLAS detector,” arXiv:1302.3694 [hep-ex].
- [33] M. S. Carena, J. R. Espinosa, M. Quiros and C. E. M. Wagner, “Analytical expressions for radiatively corrected Higgs masses and couplings in the MSSM,” Phys. Lett. B **355**, 209 (1995) [hep-ph/9504316]; M. S. Carena, M. Quiros and C. E. M. Wagner, “Effective potential methods and the Higgs mass spectrum in the MSSM,” Nucl. Phys. B **461**, 407 (1996) [hep-ph/9508343].
- [34] M. Lungwitz, “Search for third generation squarks with the ATLAS detector,” ATLAS-PROC-2012-215.
- [35] S. Heinemeyer, O. Stal and G. Weiglein, “Interpreting the LHC Higgs Search Results in the MSSM,” Phys. Lett. B **710** (2012) 201 [arXiv:1112.3026 [hep-ph]]; N. D. Christensen, T. Han and S. Su, “MSSM Higgs Bosons at The LHC,” Phys. Rev. D **85** (2012) 115018 [arXiv:1203.3207 [hep-ph]]; R. Benbrik, M. Gomez Bock, S. Heinemeyer, O. Stal, G. Weiglein and L. Zeune, “Confronting the MSSM and the NMSSM with the Discovery of a Signal in the two Photon Channel at the LHC,” Eur. Phys. J. C **72** (2012) 2171 [arXiv:1207.1096 [hep-ph]]; A. Arbey, M. Battaglia, A. Djouadi and F. Mahmoudi, “The Higgs sector of the phenomenological MSSM in the light of the Higgs boson discovery,” JHEP **1209** (2012) 107 [arXiv:1207.1348 [hep-ph]]; M. Drees, “A Supersymmetric Explanation of the Excess of Higgs-Like Events at the LHC and at LEP,” Phys. Rev. D **86** (2012) 115018 [arXiv:1210.6507 [hep-ph]].
- [36] M. S. Carena, S. Mrenna and C. E. M. Wagner, “MSSM Higgs boson phenomenology at the Tevatron collider,” Phys. Rev. D **60**, 075010 (1999) [hep-ph/9808312].
- [37] J. R. Ellis, M. K. Gaillard and D. V. Nanopoulos, “A Phenomenological Profile of the Higgs Boson,” Nucl. Phys. B **106** (1976) 292.

- [38] M. A. Shifman, A. I. Vainshtein, M. B. Voloshin and V. I. Zakharov, “Low-Energy Theorems for Higgs Boson Couplings to Photons,” *Sov. J. Nucl. Phys.* **30** (1979) 711 [*Yad. Fiz.* **30** (1979) 1368].
- [39] M. Carena, G. Nardini, M. Quiros and C. E. M. Wagner, “MSSM Electroweak Baryogenesis and LHC Data,” *JHEP* **1302** (2013) 001 [arXiv:1207.6330 [hep-ph]].
- [40] A. Denner, S. Heinemeyer, I. Puljak, D. Rebuzzi and M. Spira, “Standard Model Higgs-Boson Branching Ratios with Uncertainties,” *Eur. Phys. J. C* **71** (2011) 1753 [arXiv:1107.5909 [hep-ph]].
- [41] J. R. Espinosa, C. Grojean, M. Muhlleitner and M. Trott, “Fingerprinting Higgs Suspects at the LHC,” *JHEP* **1205** (2012) 097 [arXiv:1202.3697 [hep-ph]].
- [42] A. Djouadi, “The Anatomy of electro-weak symmetry breaking. II. The Higgs bosons in the minimal supersymmetric model,” *Phys. Rept.* **459** (2008) 1 [hep-ph/0503173].
- [43] See e.g. Conference talks in ”Fourth International Workshop in Prospects for Charged Higgs Discovery at Colliders”, Uppsala University, Sweden, 8-11 October 2012, <http://www.grid.tsl.uu.se/chargedhiggs2012/>.